

MIP-plicits: Level of Detail Factorization of Neural Implicits Sphere Tracing

Vinícius da Silva
Guilherme Schardong
Hélio Lopes

vinicius.silva@exacta.inf.puc-rio.br
gschardong@inf.puc-rio.br
lopes@inf.puc-rio.br
PUC-Rio
Rio de Janeiro, RJ, Brazil

Tiago Novello

Luiz Velho

tiago.novello@impa.br

lvelho@impa.br

National Institute for Pure and
Applied Mathematics (IMPA)
Rio de Janeiro, RJ, Brazil

Luiz Schirmer

luiz.schirmer@isr.uc.pt

Institute of Systems and Robotics -
University of Coimbra
Coimbra, Coimbra, Portugal

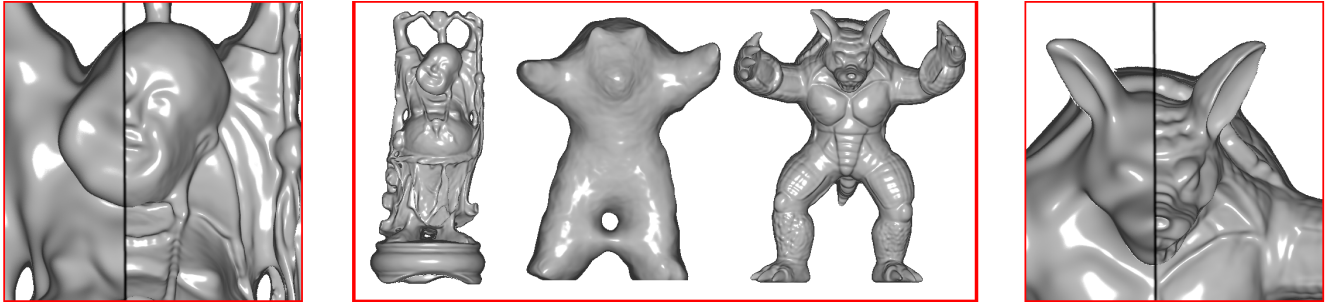


Figure 1: MIP-plicits applying Neural Implicit Normal Mapping. In the middle, a 4D case morphing the Happy Buddha into the Armadillo. On the left and right, 3D close-ups with and without Neural Implicit Normal Mapping enabled side-by-side.

ABSTRACT

We introduce MIP-plicits, a novel approach for rendering 3D and 4D Neural Implicits that divide the problem into macro and meso components. We rely on the iterative nature of the sphere tracing algorithm, the spatial continuity of the Neural Implicit representation, and the association of the network architecture complexity with the details it can represent. This approach does not rely on spatial data structures, and can be used to mix Neural Implicits trained previously and separately as detail levels.

We also introduce Neural Implicit Normal Mapping, which is a core component of the problem factorization. This concept is very close and analogous to the classic normal mapping on meshes, broadly used in Computer Graphics.

Finally, we derive an analytic equation and an algorithm to simplify the normal calculation of Neural Implicits, adapted to be evaluated by the General Matrix Multiply algorithm (GEMM). Current approaches rely on finite differences, which impose additional inferences on auxiliary points and discretization error.

CCS CONCEPTS

• Computing methodologies → Ray tracing; Neural networks.

KEYWORDS

neural implicits, sphere tracing, normal mapping

ACM Reference Format:

Vinícius da Silva, Guilherme Schardong, Hélio Lopes, Tiago Novello, Luiz Velho, and Luiz Schirmer. 2022. MIP-plicits: Level of Detail Factorization of Neural Implicits Sphere Tracing. In *Proceedings of (C'18)*. ACM, New York, NY, USA, 8 pages. <https://doi.org/10.1145/nnnnnnnn.nnnnnnnn>

1 INTRODUCTION

Neural Implicits (NI) have emerged as a model representation in Computer Graphics. They consist of Neural Networks representing Signed Distance Functions (SDFs) of implicit surfaces, which can be rendered finding their level sets. An approach broadly used for this visualization task is the Sphere Tracing (ST) algorithm [13, 14].

NIs opened an avenue of research challenges for exploration, including how to flexibly render them. Previous approaches train specific spatial data-structures, which can be inflexible and restrictive workflow-wise. Another option is to extract the level sets using Marching Cubes, which is slow, results in meshes that require much more storage than NIs, and depends on grid resolution.

We propose *MIP-plicits*, a novel approach that factorizes *Neural Implicit Sphere Tracing* into *macro* and *meso* components. The macro component is the novel *Multiscale Sphere Tracing* operating on a sequence of NIs, each one having higher representation capacity than the previous. The meso component is represented by a novel

Permission to make digital or hard copies of all or part of this work for personal or classroom use is granted without fee provided that copies are not made or distributed for profit or commercial advantage and that copies bear this notice and the full citation on the first page. Copyrights for components of this work owned by others than ACM must be honored. Abstracting with credit is permitted. To copy otherwise, or republish, to post on servers or to redistribute to lists, requires prior specific permission and/or a fee. Request permissions from permissions@acm.org.

C'18,
© 2022 Association for Computing Machinery.
ACM ISBN 978-x-xxxx-xxxx-x/YY/MM...\$15.00
<https://doi.org/10.1145/nnnnnnnn.nnnnnnnn>

Neural Implicit Normal Mapping, which maps the gradient of a finer NI to the output of the Multiscale Sphere Tracing.

MIP-plicits enable real-time rendering of NIs, without the use of spatial data structures. This allows the algorithm to work with 3D and 4D (3D plus time) previously trained NIs, integrating them as detail levels. Our *contributions* include:

- Multiscale Sphere Tracing;
- Real-time rendering of 3D and 4D NIs;
- Level of Detail without spatial data-structures;
- Can use previously trained NIs as detail levels;
- Neural Implicit Normal Mapping;
- Analytic equation and algorithm for normal calculation.

2 RELATED WORK

2.1 Signed Distance Functions

The use of implicit functions to describe surfaces is an essential topic in computer graphics [29]. In particular, SDFs compose an important class of implicit functions which encode the surfaces on their zero-level sets [2] and arise from solving the Eikonal problem [26].

Recently, neural networks are being used to represent SDFs through NIs [12, 25, 27]. In general, NIs use *multilayer perceptrons networks* (MLP) with a nonlinear activation function to represent implicit functions. *Sinusoidal networks* are an important example, which uses the sine as the activation function. They are suitable for reconstructing signals and can approximate all continuous functions in the cube [8]. We use the NI framework described in [23] which considers the network initialization given in [27].

2.2 Visualization of SDF level sets

Marching cubes [16, 20] and *sphere tracing* [13, 14] are classical visualization methods for rendering SDF level sets. Marching cubes extracts level sets as meshes for visualization, and sphere tracing renders the surface by iterating points along the view rays. Neural versions of those algorithms can also be found in [4, 17, 19].

The initial works in NIs use marching cubes to generate visualizations of the resulting level sets [12, 25, 27]. Recent works have been focusing on sphere tracing, since no intermediary representation is needed for rendering [9, 28]. We take the same path.

Fast inference is needed to sphere trace NIs level sets. Davies et al. [9] shows that this is possible on rendering using the General Matrix Multiply (GEMM) algorithm [10, 22], but the capacity of the networks used in that work does not seem to represent geometric detail. We are using the NI framework in [23] which allows us to represent fine detailed geometry. We also propose to use the continuity property of the SDFs to train multiple networks of the same geometry at different configurations. We empirically show that the ST can be adapted to work with multiple NIs and that it is possible to transfer details from them in the process. Additionally, we derive a closed form for the NI gradients which can be evaluated at rendering time, improving shading performance and accuracy.

2.3 Level Of Detail

Level of detail (LOD) is a set of techniques in computer graphics used to represent a given surface by a certain number of surfaces sorted by its geometric complexity [6]. LOD techniques are common in

3D rendering. They increase the rendering efficiency by using fine models only when the camera approximates the surface. Examples includes *subdivision surfaces* [3], which considers the parametric nature of surfaces. MIP-plicits define a way to handle NIs using LOD. The definition is inspired by the classic *mipmapping* [30].

Normal mapping [5, 7] is a classic way to transfer detailed normals between meshes, inspired by *bump mapping* [1] and *displacement mapping* [15]. Besides depending on interpolation, normal mapping also suffers distortions of the parametrization between the underlying meshes, which are assumed to have the same topology. On the other hand, using the continuous properties of NIs allows us to map the gradient of a finer NI to a coarser one. This mapping considers a volumetric neighborhood of the coarse surface instead of parametrizations, and does not rely on interpolations like the classic one. We call this technique *neural implicit normal mapping*.

State-of-the-art works in NIs propose to store feature components in the nodes of *octrees* [21, 28]. Those are used to create codes, which are fed to small networks for distance inference. Octree-based approaches have the drawback of needing feature interpolation mechanisms. As a consequence, the resulting function is not necessarily differentiable at the voxel boundaries. This could imply in noncontinuous gradients, which may impact the shading procedure.

MIP-plicits have continuous gradients, since they use smooth NIs as LOD. Another consequence is that they can integrate previously trained models as LOD. They also do not need any spatial data-structure. Finally, MIP-plicits support time-varying 3D surfaces.

3 MIP-PLICITS

3.1 Motivation

The key idea behind MIP-plicits is exploring the iterative nature of the ST algorithm. The hypothesis is that the overhead of each iteration would be decreased if we would use coarse neural surfaces. Then, finer models can be used to fetch details.

NIs have properties that support that hypothesis. First, they are continuous, i.e., the SDFs are defined for all points in the underlying space. Second, a coarser or finer version of a NI can be defined by changing the number and size of hidden layers and training using the same data. However, questions remain about how to transit between NIs. Is this operation always defined? Is it continuous?

The ST algorithm already contains an intuition for those questions. At any iteration, it outputs points using a NI for distance inference. Note that even though those points are related to the NI domain, they are also defined in the domain of any other NI trained on the same data. Increasing the width and the depth of hidden layers for a subsequent NI allows us to represent a finer LOD with a slightly different SDF approximation.

Another question arises: can we use the inferred points as the transition between the NIs? MIP-plicits answers this. A MIP-plicit is a sequence of NIs sorted by LOD, which can be used at different iterations of the ST. As usual in this algorithm, the points inferred on the previous iteration are used as input for the next iteration, but any NI in the MIP-plicit can be used for inference.

It is important to note that transiting between SDFs was not possible for the ST algorithm before because defining LOD for general SDFs is not trivial. Given an SDF, there is no approach to systematically derive a simplified or more complex version of it.

However, this is easily done using NIs by just changing the number and size of hidden layers and training using the same data.

MIP-plicits needs an additional property for this ST to work. Since neural surfaces representing the same data are slightly different, a ray intersecting a neural surface could not intersect another surface, and vice-versa. This situation can occur in silhouette regions (see Fig. 2). We overcome this problem by requiring the finer surface to be inside a neighborhood of the coarse one. Then we sphere trace the boundary of this neighborhood and continue the ST using the finer NI. Finally, we simplify the stop condition to use a fixed number of iterations instead of a distance threshold. This avoids thread divergence, which can be harmful for parallelism (nonetheless other adaptive strategies can be used).

3.2 Definition

A *Neural Implicit* (NI) is a smooth function $f_\theta : \mathbb{R}^3 \rightarrow \mathbb{R}$ represented by a neural network such that $|\nabla f_\theta| \approx 1$. We consider f_θ to be a *multilayer perceptron network* with $n - 1$ hidden layers:

$$f_\theta(p) = W_n \circ f_{n-1} \circ f_{n-2} \circ \dots \circ f_0(p) + b_n, \quad (1)$$

where $f_i(p_i) = \varphi(W_i p_i + b_i)$ is the i -layer obtained by applying a smooth *activation function* $\varphi : \mathbb{R} \rightarrow \mathbb{R}$ to each coordinate of the affine map given by the linear transformation $W_i : \mathbb{R}^{N_i} \rightarrow \mathbb{R}^{N_{i+1}}$ translated by the *bias* $b_i \in \mathbb{R}^{N_{i+1}}$. The union of their coefficients correspond to the parameters θ of f_θ . We call the zero-level set $f_\theta^{-1}(0)$ a *neural surface* and denote it by S_θ .

Let f_{θ_1} and f_{θ_2} be NIs trained on the same data. We say that f_{θ_1} has *less detail* than f_{θ_2} , and denote it by $f_{\theta_1} \triangleright f_{\theta_2}$, if the network f_{θ_2} has more capacity than f_{θ_1} , and there is a neighborhood of the neural surface S_{θ_2} contained in a neighborhood of S_{θ_1} . In other words, there are small positive numbers ϵ_1 and ϵ_2 implying the *level of detail* (LOD) condition:

$$[|f_{\theta_1}| \leq \epsilon_1] \subset [|f_{\theta_2}| \leq \epsilon_2]. \quad (2)$$

We define a *MIP-plicit* as a sequence of NIs $f_{\theta_1} \triangleright \dots \triangleright f_{\theta_m}$ such that $f_{\theta_{j+1}}$ has more detail than f_{θ_j} for $j = 1, \dots, m-1$. We denote the corresponding neural surfaces by S_j to simplify the notation. The LOD condition implies that each neural surface S_{j+1} is contained in $[|f_{\theta_j}| \leq \epsilon_j]$. Thus, to sphere trace S_{j+1} we can first sphere trace $S_j + \epsilon_j := f_{\theta_j}^{-1}(\epsilon_j)$ then continue with $f_{\theta_{j+1}}$ (see Fig. 2).

We can also extend MIP-plicits to 4D using 1-families of NIs. More precisely, suppose that the underlying sequence of networks $f_{\theta_1}, \dots, f_{\theta_m}$ has the *space-time* $\mathbb{R}^3 \times \mathbb{R}$ as domain. That is, each network is a 1-family of NIs $f_{\theta_j}(\cdot, t) : \mathbb{R}^3 \rightarrow \mathbb{R}$ indexed by $t \in \mathbb{R}$. Then, we require the sequence of NIs $f_{\theta_1}(\cdot, t) \triangleright \dots \triangleright f_{\theta_m}(\cdot, t)$ to be a MIP-plicit, for each $t \in \mathbb{R}$. See [24] for more details on families of NIs. Varying t animates the initial MIP-plicit $f_{\theta_1}(\cdot, 0) \triangleright \dots \triangleright f_{\theta_m}(\cdot, 0)$, resulting in a 1-family of MIP-plicits.

Next, given a MIP-plicit $f_{\theta_1} \triangleright \dots \triangleright f_{\theta_m}$ we provide a *Multiscale ST algorithm* that operates on $f_{\theta_1} \triangleright \dots \triangleright f_{\theta_{m-1}}$ and a *neural implicit normal mapping* that transfer the gradient of f_{θ_m} to the ST output.

4 MULTISCALE SPHERE TRACING

Let $f_{\theta_1} \triangleright \dots \triangleright f_{\theta_m}$ be a MIP-plicit, p_0 be a point outside $[|f_{\theta_1}| \leq \epsilon_1]$, and v be a direction. We define a Multiscale ST that approximates the first hit between the ray $\gamma(t) = p_0 + tv$, with $t > 0$, and the neural

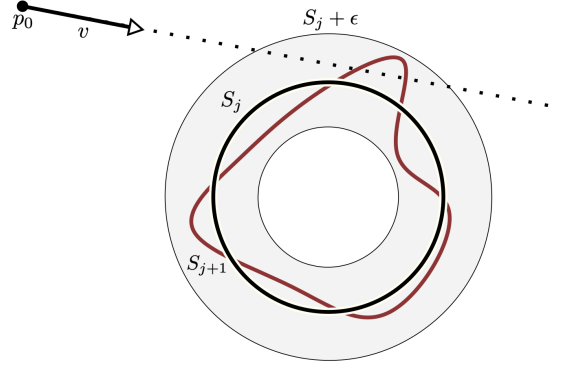


Figure 2: Illustration of a ray intersecting a pair of neural surfaces S_j and S_{j+1} with their NIs satisfying $f_{\theta_j} \triangleright f_{\theta_{j+1}}$.

surface S_{m-1} . More precisely, let $0 = n_0 < n_1 < \dots < n_{m-1} = n$ be a sequence where $n_j - n_{j-1}$ will be the number of ST iterations using f_{θ_j} . The first intersection between γ and S_{m-1} can be computed iterating $p_{i+1} = p_i + f_{\theta_j}(p_i)v$, with $n_{j-1} \leq i < n_j$. In the 4D case, the algorithm operates in 1-families of MIP-plicits indexed by an additional time parameter. We use the finer NI f_{θ_m} only to compute the normal $\nabla f_{\theta_m}(p_n)$ at p_n , in the neural implicit normal mapping (Sec. 5). The Multiscale ST is shown in Algorithm 1.

ALGORITHM 1: Multiscale ST algorithm

Input: A MIP-plicit $f_{\theta_1} \triangleright \dots \triangleright f_{\theta_{m-1}}$, position p_0 , unit direction v , number of accumulated iterations $n_1 < \dots < n_{m-1}$

Output: End point p_n

```

1 for  $j = 1, \dots, m-1$  do
2   for  $i = n_{j-1}, \dots, n_j$  do
3     if  $j = m-1$  then
4        $p_{i+1} = p_i + f_{\theta_j}(p_i)v$ ;
5     else
6        $p_{i+1} = p_i + (f_{\theta_j}(p_i) - \epsilon_j)v$ ;
7     end
8   end
9 end
```

If $\gamma \cap S_{m-1} \neq \emptyset$, the Multiscale ST approximates the first hit point q between the ray γ and the neural surface S_{m-1} . Indeed, by the LOD condition, if $\gamma \cap (S_j + \epsilon_j) \neq \emptyset$ implies $\gamma \cap (S_{j-1} + \epsilon_{j-1}) \neq \emptyset$. Using an appropriate n_j , the classical ST guarantees that $p_{i+1} = p_i + f_{\theta_j}(p_i)v$, with $n_{j-1} \leq i < n_j$, approximates the intersection between γ and $S_j + \epsilon_j$. Therefore, the proof of the claim follows by induction.

For the inference of a NI, required in line 4 of Algorithm 1, we use the GEMM algorithm [10] for each layer, an approach used for low-abstraction-level implementation of multilayer perceptrons.

The final step for rendering is to calculate the normals, given by the gradients of the final NI. This enables the use of shading models. The next section describes the process.

5 NEURAL IMPLICIT NORMAL MAPPING

In previous works finite differences have been used to approximate normals for NI rendering. Even though this approach works, it

comes with drawbacks, such as the necessity of additional inferences on auxiliary points, and the error imposed by discretization.

We can use MIP-plicits and the analytical equation described in [23] to overcome that problem. The idea is to use the most capable NI (f_{θ_m}) in the underlying MIP-plicit to fetch the normals. Analogously to the classic normal mapping, which maps detailed normals stored in textures to meshes via UV-coordinates, neural implicit normal mapping transfers detailed gradients in a neighborhood of the finer neural surface S_m to S_{m-1} via the output points of the Multiscale ST. This procedure is well defined because the LOD condition (Eq. 2) holds, i.e. $f_{\theta_{m-1}} \triangleright f_{\theta_m}$.

We can compute the gradient of a NI f_{θ} explicitly using

$$\nabla f_{\theta}(p) = W_n \cdot \mathbf{J}f_{n-1}(p_{n-1}) \cdot \dots \cdot \mathbf{J}f_1(p_1) \cdot \mathbf{J}f_0(p). \quad (3)$$

Where \mathbf{J} is the *Jacobian* and $p_i = f_{i-1} \circ \dots \circ f_0(p)$. The Jacobians of the functions f_i applied to the points p_i are given by:

$$\mathbf{J}f_i(p_i) = W_i \odot \varphi' [a_i | \dots | a_i] \quad (4)$$

where \odot is the *Hadamard* product, and the matrix $[a_i | \dots | a_i]$ has N_i copies of the vector $a_i = W_i(p_i) + b_i \in \mathbb{R}^{N_{i+1}}$.

In the 4D case, the neural implicit normal map applies the gradient of $f_{\theta_m}(\cdot, t)$ to the output of the ST algorithm.

6 ANALYTIC NORMAL CALCULATION FOR THE GEMM ALGORITHM

The normals of a neural surface are given by the gradient of its NI f_{θ} . This is represented by Equation 3 which is a sequence of matrix multiplications, one for each layer of f_{θ} . Observe that these multiplications do not fit into a (parallel) GEMM setting directly since the first matrix $\mathbf{J}f_0(p)$ belongs to $\mathbb{R}^{3 \times N_1}$. This is a problem because the GEMM algorithm organizes the input points into a matrix, where its lines correspond to the point coordinates and its columns organize the points and enable parallelism. However, we can solve this problem using three GEMMs, one for each normal coordinate. Thus, each GEMM starts with a column of $\mathbf{J}f_0(p)$ eliminating one of the dimensions. Notice that the resulting multiplications can be asynchronous, since they are completely independent.

Specifically, let $f_{\theta} : \mathbb{R}^3 \rightarrow \mathbb{R}$ be a NI with $n - 1$ hidden layers, as defined in Equation 1. The j -coordinate of the gradient $\nabla f_{\theta}(p)$ at a point p is given by $G_n = W_n \cdot G_{n-1}$, where G_{n-1} is obtained by iterating the system $G_i = \mathbf{J}f_i(p_i) \cdot G_{i-1}$ for $i = 1, \dots, n - 1$, with the initial condition $G_0 = W_0[j] \odot \varphi'(a_0)$. The vector $W_0[j]$ denotes the j -column of the weight matrix W_0 .

The calculations of G_0 and G_n are straightforward and can be solved using a kernel and a GEMM. To compute the term G_i for $i = 1, \dots, n - 1$, observe that

$$G_i = \left(W_i \odot \varphi' [a_i | \dots | a_i] \right) \cdot G_{i-1} = (W_i \cdot G_{i-1}) \odot \varphi'(a_i).$$

The first equality comes from Equation 4 and the second is a consequence of a kind of commutative property of the Hadamard product and can be easily verified. The second expression needs fewer computations and can be solved using a GEMM followed by a kernel.

Algorithm 2 presents the above gradient computation for a batch of points. The input is a matrix $P \in \mathbb{R}^{3 \times k}$, where its columns correspond to k points generated by the GEMM version of Algorithm 1. The algorithm outputs a matrix $\nabla f_{\theta}(P) \in \mathbb{R}^{3 \times k}$, where its j -column

is the gradient of f_{θ} evaluated at the point $P[j]$. The output vector G_n for $j = 0, 1, 2$, in line 16, composes the three lines of $\nabla f_{\theta}(P)$.

Lines 2–5 are responsible for computing G_0 , lines 6–11 compute G_{n-1} , and line 13 provides the result G_n . Note that we are abusing the notation in line 3 because we are considering that the operation $W_0 \cdot P + b_0$ is summing b_0 to each column of $W_0 \cdot P$.

ALGORITHM 2: Normal computation

```

Input: NI  $f_{\theta}$ , positions  $P$ 
Output: Gradients  $\nabla f_{\theta}(P)$ 
1 for  $j = 0$  to 2 (async) do
    // Input Layer
2   using a GEMM:
3    $A_0 = W_0 \cdot P + b_0$ 
4   using a kernel:
5    $G_0 = W_0[j] \odot \varphi'(A_0); P_0 = \varphi(A_0)$ 

    // Hidden layers
6   for layer  $i = 1$  to  $n - 1$  do
7     using GEMMs:
8      $A_i = W_i \cdot P_{i-1} + b_i; G_i = W_i \cdot G_{i-1}$ 
9     using a kernel:
10     $G_i = G_i \odot \varphi'(A_i); P_i = \varphi(A_i)$ 
11  end

    // Output layer
12  using a GEMM:
13   $G_n = W_n \cdot G_{n-1}$ 
14 end
```

7 EXPERIMENTS

We evaluate MIP-plicits using NIs as defined in Equation (1), and we choose the sine as the activation function, i.e. $\varphi = \sin$. We assume NIs trained using the framework described in [23], which uses the initialization of the network given in [27]. Each LOD of a MIP-plicit is assumed to be an independent NI, trained on the same data. We use the NI with more capacity in the MIP-plicit as a baseline. The Multiscale ST algorithm is fixed at 20 iterations. The renderer is implemented on CUDA, and GEMMs are evaluated using the CUTLASS library for the MIP-plicits and the baselines. All images are 512×512 . No acceleration structures or bounding boxes are used, so all pixels are evaluated. The Phong lighting model is used. All experiments are conducted on a NVidia Geforce RTX 3090.

We use a simplified notation to refer to network architectures. For example, $(64, 1) \triangleright (256, 3)$ means a MIP-plicit with a network with one 64×64 matrix (i.e. 2 hidden layers with 64 neurons) for the Multiscale ST, and a network with three 256×256 matrices (i.e. 4 hidden layers with 256 neurons) for the Neural Implicit Normal Mapping. Another example: $(64, 1)$ (without an additional Level of Detail) means that the same architecture is used for both the Multiscale ST algorithm and the normal calculation.

The first experiment evaluates image quality and performance for 3D datasets. We evaluate models from the Stanford repository, namely Bunny, Dragon, Happy Buddha, and Lucy. Figure 3 shows how Neural Implicit Normal Mapping increases fidelity, using the

Happy Buddha as example. Figure 5 is a broader rendering evaluation of the models, comparing several MIP-plicit configurations with the baseline. Table 1 shows the quantitative comparisons.



Figure 3: Neural Implicit Normal Mapping of the Happy Buddha. On the left, a (64, 1) NI without normals mapped. On the right, a MIP-plicit mapping the normals of the (256, 3) NI into the (64, 1) NI.

Table 1: MIP-plicit configuration comparison. Models with the same configuration perform equally.

MIP-plicit	FPS	Speedup	Memory (KB)
baseline	19.7	1.0	777
(64, 1)	122.0	6.2	18
(64, 1) ▷ (256, 1)	70.0	3.6	281
(64, 1) ▷ (256, 2)	52.0	2.6	538
(64, 1) ▷ (256, 3)	40.5	2.1	795

Notice how MIP-plicits are very flexible regarding the tradeoff between image quality, performance and memory usage. On one hand, a (64, 1) configuration can be used when fidelity is not necessary, resulting in a high framerate (122 FPS). On the other hand, the (64, 1) ▷ (256, 1) configuration is a good tradeoff between performance and fidelity since it is near to the baseline, but performs 3.6 times faster. If more details are needed, (64, 1) ▷ (256, 2) or (64, 1) ▷ (256, 3) can be used. Remember that the baseline already has good performance, since it uses a fast GEMM-based inference renderer implemented in CUDA and CUTLASS.

We should analyse the simplest MIP-plicit configuration with one NI for the Multiscale ST and another for the Neural Implicit Normal Mapping, which is the most effective in our tests. Differently

from classical normal mapping, Neural Implicit Normal Mapping is volumetric. Thus, it cannot suffer from projection distortion. It also does not require any manual tweaking of the normals. However, this configuration has one limitation: it tends to darken the silhouette of objects, a consequence of the slightly different surfaces that the NIs composing the MIP-plicit represent. This phenomenon is evaluated in the second experiment (Figure 4). It compares the (64, 1) ▷ (256, 3) and (64, 1) ▷ (256, 2) ▷ (256, 3) configurations. Adding one level of detail for the Multiscale ST helps with the silhouette, at a slight expense of performance. The number of iterations still 20 for the Multiscale ST, but 3 were used for the first level and 17 for the second level. This case runs at 25 FPS.

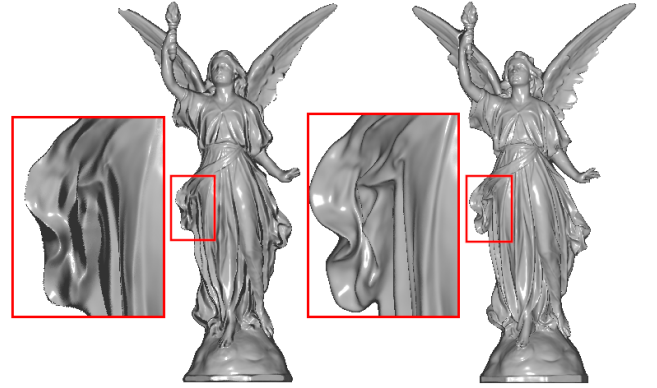


Figure 4: Silhouette evaluation on Lucy. From left to right: (64, 1) ▷ (256, 3), and (64, 1) ▷ (256, 2) ▷ (256, 3). Notice how the silhouettes are darkened on the left and how the additional (256, 2) level improves the result.

The third experiment evaluates a 4D MIP-plicit which morphs the Happy Buddha into the Armadillo. Figure 6 shows that MIP-plicits and Neural Implicit Normal Mapping also work in 4D. Notice, however, that the first level need more capacity because of the additional dimension. Tests with a (64, 1) ▷ (256, 3) MIP-plicit review that the (64, 1) configuration is insufficient to represent the transition properly and cannot maintain the level of detail condition (Eq. 2). The (256, 1) configuration runs at 40 FPS, the (256, 1) ▷ (256, 3) MIP-plicit at 29 FPS, and the baseline at 20 FPS.

8 CONCLUSION

We presented MIP-plicits, a novel approach to render NIs, which factorizes ST into macro and meso components. It does not use spatial data structures, supporting 3D and 4D NIs and the integration of models trained separately as detail levels. We also introduced Neural Implicit Normal Mapping, a novel way to map details between NIs, and a new way to calculate normals analytically.

MIP-plicits open paths for several future work options. For example, exploring more applications for the (attribute) mapping via 3D points generated by the ST. A core problem in this context is how to add micro components into the factorization. Possible candidates include material properties, BRDFs, textures, and hypertextures.

More exploration can also be done using other networks for LOD, both for the Multiscale ST and for attribute mapping. For example,

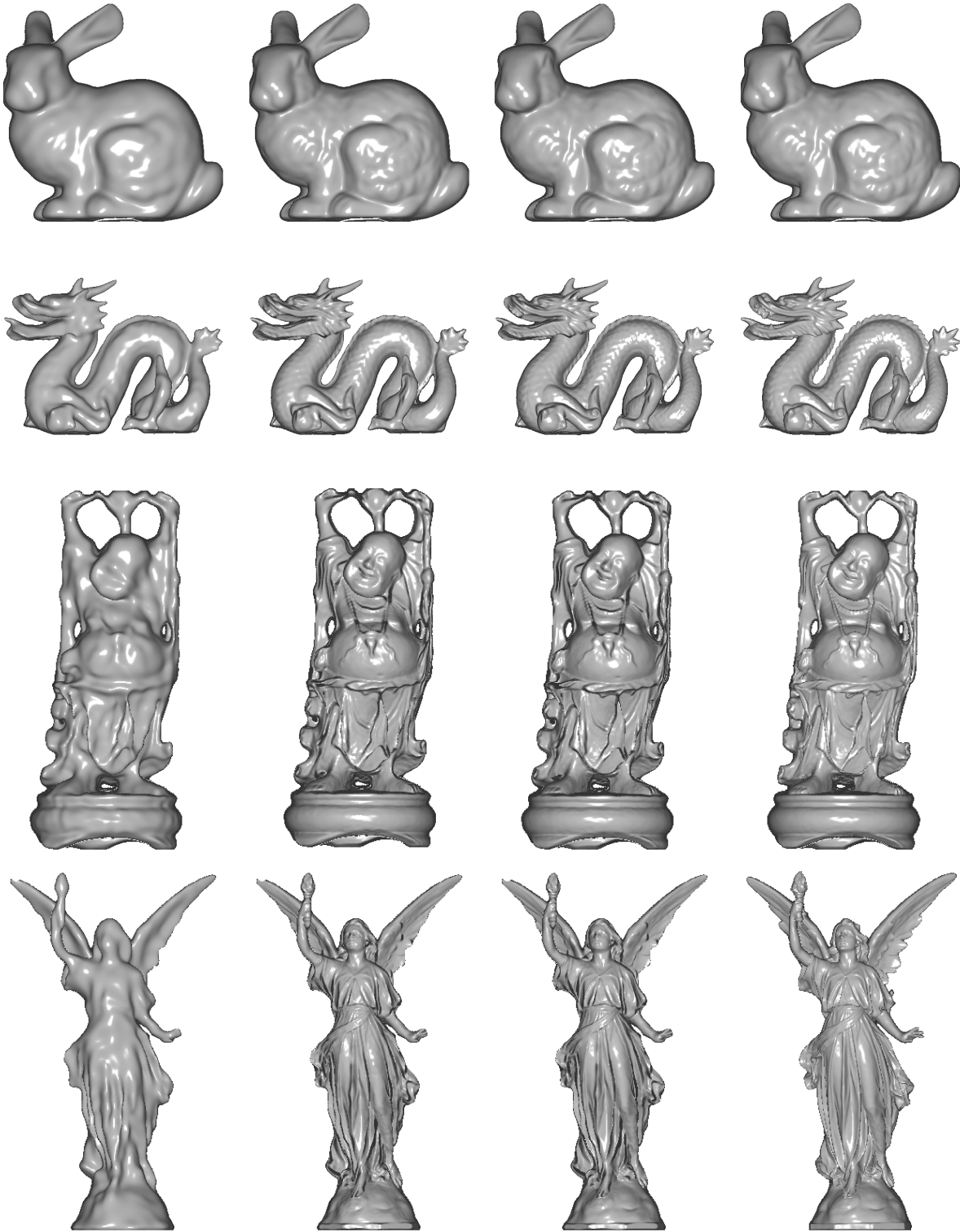


Figure 5: Comparison between MIP-plicit configurations and the baseline. The columns represent different configurations. From left to right: (64, 1), (64, 1) \triangleright (256, 1) (Bunny and Dragon) and (64, 1) \triangleright (256, 2) (Happy Buddha and Lucy), (64, 1) \triangleright (256, 3), and the baseline (256, 3). Notice how the second column is already similar to the baseline. The third column adds more detail.

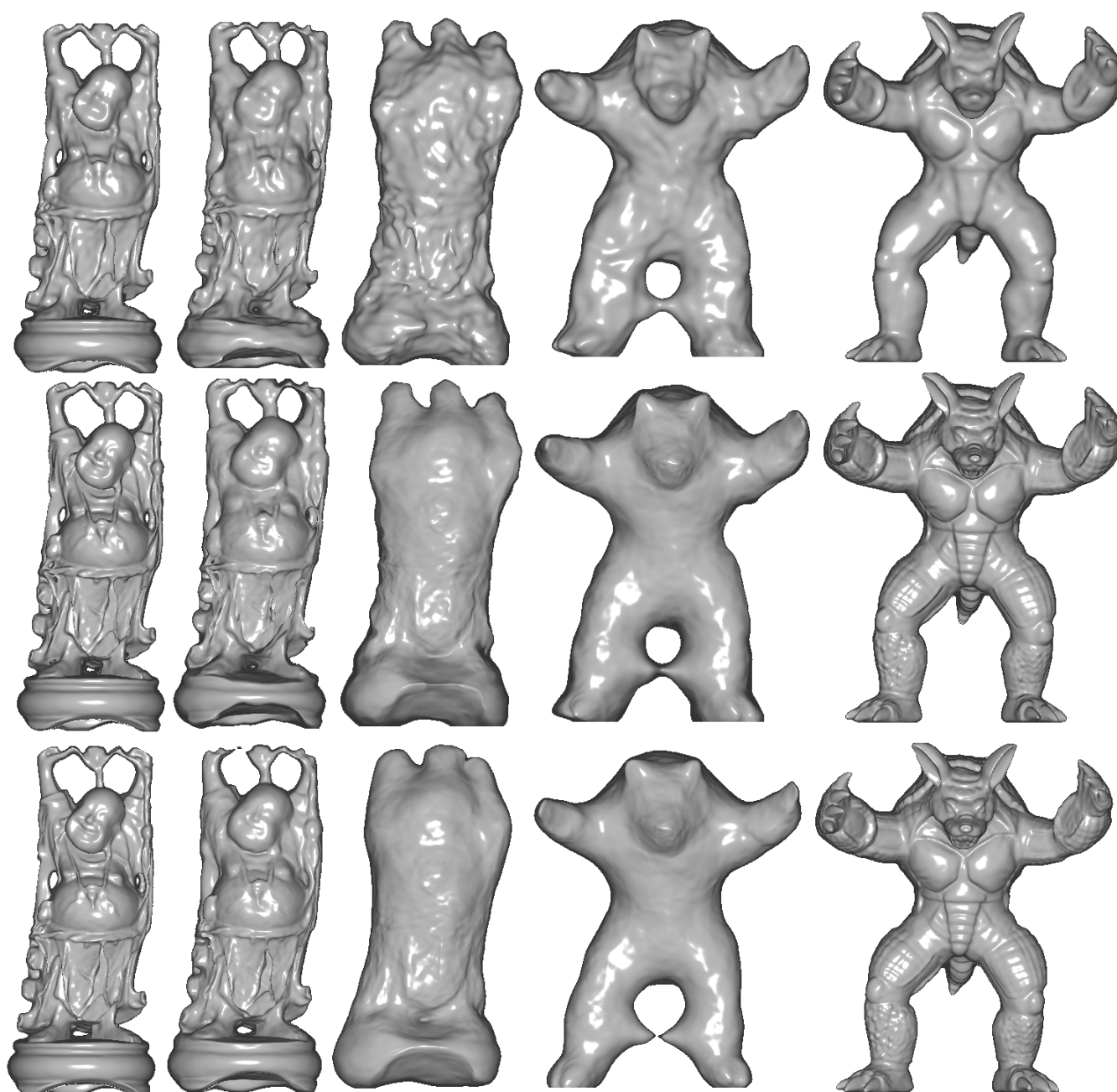


Figure 6: 4D NIs representing the morphing between the Happy Buddha and the Armadillo. From top to bottom: (256, 1), a MIP-plicit (256, 1) \triangleright (256, 3), and the baseline (256, 3). Notice how the Neural Implicit Normal Mapping in the 2nd row increases fidelity.

[11, 18] introduced *multiplicative filter networks* which allows LOD to be encoded in a single network. This network could be used in conjunction with MIP-plicits.

Another path to explore is performance. Even though MIP-plicits have realtime performance, several improvements can be done to further optimize the algorithm. For example, using fully-fused GEMMs can decrease the overhead of GEMM setup [22]. Additionally, MIP-plicits could benefit greatly from any faster new formulation of the normal computation, since it still an expensive operation to perform. MIP-plicits can also be easily adapted to work with acceleration structures and ray tracing engines such as OptiX.

REFERENCES

- [1] James F Blinn. 1978. Simulation of wrinkled surfaces. *ACM SIGGRAPH computer graphics* 12, 3 (1978), 286–292.
- [2] Jules Bloomenthal and Brian Wyvill. 1990. Interactive techniques for implicit modeling. *ACM Siggraph Computer Graphics* 24, 2 (1990), 109–116.
- [3] Edwin Earl Catmull. 1974. *A subdivision algorithm for computer display of curved surfaces*. The University of Utah.
- [4] Zhiqin Chen and Hao Zhang. 2021. Neural Marching Cubes. *ACM Trans. Graph.* 40, 6, Article 251 (dec 2021), 15 pages. <https://doi.org/10.1145/3478513.3480518>
- [5] Paolo Cignoni, Claudio Montani, Claudio Rocchini, and Roberto Scopigno. 1998. A general method for preserving attribute values on simplified meshes. In *Proceedings Visualization '98 (Cat. No. 98CB36276)*. IEEE, 59–66.
- [6] James H Clark. 1976. Hierarchical geometric models for visible surface algorithms. *Commun. ACM* 19, 10 (1976), 547–554.
- [7] Jonathan Cohen, Marc Olano, and Dinesh Manocha. 1998. Appearance-preserving simplification. In *Proceedings of the 25th annual conference on Computer graphics and interactive techniques*. 115–122.
- [8] George Cybenko. 1989. Approximation by superpositions of a sigmoidal function. *Mathematics of control, signals and systems* 2, 4 (1989), 303–314.
- [9] Thomas Davies, Derek Nowrouzezahrai, and Alec Jacobson. 2020. On the Effectiveness of Weight-Encoded Neural Implicit 3D Shapes. (2020). [arXiv:2009.09808](https://arxiv.org/abs/2009.09808) <http://arxiv.org/abs/2009.09808>
- [10] Jack J Dongarra, Jeremy Du Croz, Sven Hammarling, and Iain S Duff. 1990. A set of level 3 basic linear algebra subprograms. *ACM Transactions on Mathematical Software (TOMS)* 16, 1 (1990), 1–17.
- [11] Rizal Fathony, Anit Kumar Sahu, Devin Willmott, and J Zico Kolter. 2020. Multiplicative Filter Networks. In *International Conference on Learning Representations*.
- [12] Amos Gropp, Lior Yariv, Niv Haim, Matan Atzmon, and Yaron Lipman. 2020. Implicit geometric regularization for learning shapes. *arXiv preprint arXiv:2002.10099* (2020).
- [13] John C Hart. 1996. Sphere tracing: A geometric method for the antialiased ray tracing of implicit surfaces. *The Visual Computer* 12, 10 (1996), 527–545.
- [14] John C Hart, Daniel J Sandin, and Louis H Kauffman. 1989. Ray tracing deterministic 3-D fractals. In *Proceedings of the 16th Annual Conference on Computer Graphics and Interactive Techniques*. 289–296.
- [15] Venkat Krishnamurthy and Marc Levoy. 1996. Fitting smooth surfaces to dense polygon meshes. In *Proceedings of the 23rd annual conference on Computer graphics and interactive techniques*. 313–324.
- [16] Thomas Lewiner, H lio Lopes, Ant nio Wilson Vieira, and Geovan Tavares. 2003. Efficient implementation of marching cubes' cases with topological guarantees. *Journal of graphics tools* 8, 2 (2003), 1–15.
- [17] Yiyi Liao, Simon Donne, and Andreas Geiger. 2018. Deep marching cubes: Learning explicit surface representations. In *Proceedings of the IEEE Conference on Computer Vision and Pattern Recognition*. 2916–2925.
- [18] David B. Lindell, Dave Van Veen, Jeong Joon Park, and Gordon Wetzstein. 2021. BACON: Band-limited Coordinate Networks for Multiscale Scene Representation. (2021). [arXiv:2112.04645](https://arxiv.org/abs/2112.04645) <http://arxiv.org/abs/2112.04645>
- [19] Shaohui Liu, Yinda Zhang, Songyou Peng, Boxin Shi, Marc Pollefeys, and Zhaopeng Cui. 2020. Dist: Rendering deep implicit signed distance function with differentiable sphere tracing. In *Proceedings of the IEEE/CVF Conference on Computer Vision and Pattern Recognition*. 2019–2028.
- [20] William E Lorensen and Harvey E Cline. 1987. Marching cubes: A high resolution 3D surface construction algorithm. *ACM siggraph computer graphics* 21, 4 (1987), 163–169.
- [21] Julien N. P. Martel, David B. Lindell, Connor Z. Lin, Eric R. Chan, Marco Monteiro, and Gordon Wetzstein. 2021. ACORN: Adaptive Coordinate Networks for Neural Scene Representation. *ACM Transactions on Graphics* 40, 4 (may 2021), 1–13. <https://doi.org/10.1145/3450626.3459785> [arXiv:2105.02788](https://arxiv.org/abs/2105.02788)
- [22] Thomas M ller. 2021. Tiny CUDA Neural Network Framework. <https://github.com/nvmlabs/tiny-cuda-nn>.
- [23] Tiago Novello, Vinicius da Silva, Guilherme Schardong, Luiz Schirmer, H lio Lopes, and Luiz Velho. 2022. Differentiable Neural Implicits.
- [24] Tiago Novello, Vinicius da Silva, Guilherme Schardong, Luiz Schirmer, H lio Lopes, and Luiz Velho. 2022. Neural Implicit Surfaces in Higher Dimension.
- [25] Jeong Joon Park, Peter Florence, Julian Straub, Richard Newcombe, and Steven Lovegrove. 2019. DeepSDF: Learning continuous signed distance functions for shape representation. In *Proceedings of the IEEE/CVF Conference on Computer Vision and Pattern Recognition*. 165–174.
- [26] James A Sethian and Alexander Vladimirsky. 2000. Fast methods for the Eikonal and related Hamilton–Jacobi equations on unstructured meshes. *Proceedings of the National Academy of Sciences* 97, 11 (2000), 5699–5703.
- [27] Vincent Sitzmann, Julien Martel, Alexander Bergman, David Lindell, and Gordon Wetzstein. 2020. Implicit neural representations with periodic activation functions. *Advances in Neural Information Processing Systems* 33 (2020).
- [28] Towaki Takikawa, Joey Litalien, Kangxue Yin, Karsten Kreis, Charles Loop, Derek Nowrouzezahrai, Alec Jacobson, Morgan McGuire, and Sanja Fidler. 2021. Neural geometric level of detail: Real-time rendering with implicit 3D shapes. In *Proceedings of the IEEE/CVF Conference on Computer Vision and Pattern Recognition*. 11358–11367.
- [29] Luiz Velho, Jonas Gomes, and Luiz H de Figueiredo. 2007. *Implicit objects in computer graphics*. Springer Science & Business Media.
- [30] Lance Williams. 1983. Pyramidal parametrics. In *Proceedings of the 10th annual conference on Computer graphics and interactive techniques*. 1–11.